

1           **Assessing progressive mechanical instability of**  
2           **submarine slopes caused by methane hydrate**  
3           **dissociation**

4           **Jiangzhi Chen<sup>1</sup> and Shenghua Mei<sup>1</sup> and Dawei Wang<sup>1</sup> and Jin Sun<sup>1</sup> and Yue**  
5           **Sun<sup>1</sup>**

6           <sup>1</sup>Institute of Deep-Sea Science and Engineering, Chinese Academy of Sciences

7           **Key Points:**

- 8           • Gas hydrates on continental slopes may trigger submarine landslides, which poses  
9           a major threat for offshore infrastructures.  
10          • Conventional infinite slope analysis neglects finite rupture that might progressively  
11          escalate to catastrophic landslides.  
12          • Numerical model integrating slip nucleation and gas hydrate dissociation is de-  
13          veloped to link gas hydrate dissociation and landslides.  
14          • Progressive failure can be induced by minor changes in gas hydrates, influenced  
15          by failure surface depth and sediment characteristics.

---

Corresponding author: Dawei Wang, wangdawei@idsse.ac.cn

## 16 **Abstract**

17 Large amounts of gas hydrates exist on continental slopes, and pose a significant risk of  
18 triggering submarine landslides, subsequently impacting offshore infrastructures. While  
19 the infinite slope model is widely used for submarine slope stability analysis, it overlooks  
20 the potential for initial small failures to develop into large landslides. Our study inte-  
21 grates slip nucleation with excess pore pressure during gas hydrate dissociation, estab-  
22 lishing a model for progressive slope failure triggered by hydrate dissociation. Focusing  
23 on the Shenhu hydrate site GMGS3-W19, our results show that even 1% gas hydrate dis-  
24 sociation contributing to about 1 MPa overpressure can induce progressive landslides.  
25 Notably, deeper failure surfaces with gentler slopes and collapsible sediments require higher  
26 pore pressures to induce progressive failure, reducing the risk of developing into catas-  
27 trophic landslides. The results indicate that the infinite slope model may overestimate  
28 slope stability, and that submarine landslides caused by progressive failure may occur  
29 on slopes previously considered stable, such as the Ursa Basin in the northern Gulf of  
30 Mexico. This extension of the infinite slope model sheds light on potential limitations  
31 in current stability assessments, providing crucial insights for submarine landslide stud-  
32 ies and offshore infrastructure development.

## 33 **Plain Language Summary**

34 Understanding the stability of submarine slopes is crucial for assessing the risks as-  
35 sociated with submarine landslides, particularly for safeguarding offshore structures. How-  
36 ever, commonly used models, like the infinite slope model, often overlook the potential  
37 for small initial failures to escalate into larger, more significant collapses over time. This  
38 study introduces an innovative approach by integrating different models to explore how  
39 changes in gas hydrate conditions might influence slope stability. Our investigation fo-  
40 cused on Shenhu Site GMGS3-W19 revealed a surprising observation: even minor alter-  
41 ations in gas hydrate conditions can trigger substantial landslides. Furthermore, our find-  
42 ings suggest that with softer underlying materials at greater depths below seafloor, buried  
43 slopes require higher pressures to reach failure.

44 This research highlights a notable limitation in current slope stability models: their  
45 tendency to underestimate slope vulnerability, disregarding the possibility of substan-  
46 tial landslides for regions such as the Ursa Basin. By identifying these limitations, our  
47 study aims to provide valuable insights for researchers and engineers involved in subma-  
48 rine landslide studies and offshore infrastructure development. In summary, our novel  
49 approach to assessing slope stability prompts a reevaluation of conventional methods,  
50 potentially enhancing the accuracy of assessing submarine slope safety and bolstering  
51 the resilience of offshore installations.

## 52 **1 Introduction**

53 Gas hydrates are ice-like crystals in which guest molecules such as methane or car-  
54 bon dioxide are trapped in cages formed by water molecules. These hydrates remain sta-  
55 ble under low-temperature and high-pressure conditions, and are mainly stored in per-  
56 mafrost on land or in marine sediments (Ginsburg et al., 1995). The amount of methane  
57 hydrate stored in marine sediments is estimated to be  $\sim 10^4$  Gt (Kvenvolden, 1988), and  
58 has attracted increasing attention as a possible energy source. Submarine methane hy-  
59 drate deposits exist mainly on the continental slope in the hydrate stability zone, a re-  
60 gion defined by the hydrate-gas phase boundary and the bulk geothermal temperature  
61 profile (Kvenvolden, 1988; Sloan & Koh, 2007), and the base of the hydrate stability zone  
62 (BHSZ) in the bulk state is uniquely determined by the three-phase equilibrium of the  
63 hydrate phase, free gas phase and dissolved methane phases, depending on the temper-  
64 ature, pressure, and salinity. Despite being a promising energy source, methane hydrate  
65 is also a submarine geohazard that threatens offshore infrastructure, including platforms,

66 pipelines, and power and telecommunications cables, because natural or anthropogenic  
 67 perturbations in the temperature and the pressure can cause the hydrate to dissociate,  
 68 alter the stability of sediments, and lead to gas escape, sediment collapse, or even land-  
 69 slides on the continental slope (Maslin et al., 2010).

70 Among the factors that can contribute to submarine landslides, such as earthquakes,  
 71 sea-level change (e.g., Lafuerza et al., 2012; Berndt et al., 2012; Riboulot et al., 2013;  
 72 Smith et al., 2013; Brothers et al., 2013) or iceberg collision (Normandeau et al., 2021),  
 73 gas hydrate dissociation poses a more imminent risk because gas hydrates are ubiqui-  
 74 tous in the marine sediments, and the dissociation can be triggered by small perturba-  
 75 tions in the temperature and the pressure. For example, the Storegga Slide on the Nor-  
 76 wegian continental shelf, one of the largest known submarine landslides, is widely believed  
 77 to have been triggered by hydrate dissociation (Sultan et al., 2004; Brown et al., 2006).  
 78 Mechanically, the instability of the continental slope can be caused by an increase in the  
 79 shear stress of the overlying layer or by a decrease in the strength of the slope. Since the  
 80 weight of the overburden, the frictional properties, and the sediment cohesion remain rel-  
 81 atively unchanged in the short term, the stability of the slope is primarily determined  
 82 by the elevated pore pressure during the hydrate dissociation.

83 Submarine landslides on continental slopes are considered to occur on a rupture  
 84 surface with a depth much smaller than its length, and infinite slope analysis is typically  
 85 invoked to assess the slope stability. For gas hydrate-related landslides, the stability at  
 86 the potential slip surface (usually assumed to be the BHSZ) is assessed using the safety  
 87 factor  $F_S$ , i.e., the ratio of the frictional resistance at the slip surface to the shear stress  
 88 of the overlying layer (e.g., Kayen & Lee, 1991; Sultan et al., 2004; Nixon & Grozic, 2007).  
 89 Although the infinite slope model is widely used, the validity of the safety factor relies  
 90 on some simplified assumptions. The model assumes that the BHSZ is where the slip starts,  
 91 and that hydrate dissociation occurs simultaneously over the entire potential slip sur-  
 92 face. The entire slope is assumed to have homogeneous sediment and frictional proper-  
 93 ties. Some researchers have attempted to relax the assumptions by allowing the slip sur-  
 94 face not to coincide with the BHSZ (e.g., Sultan et al., 2004), but these models still as-  
 95 sume homogeneous frictional properties. Most importantly, the infinite slope model and  
 96 its modified versions, however, neglect the possibility that hydrate may dissociate at cer-  
 97 tain small finite region on the surface, and then the slip nucleates and progressively de-  
 98 velops into a large-scale catastrophic landslide.

99 In this study, we combine the excess pore pressure with the slip nucleation model  
 100 by Viesca and Rice (2012) and develop a model of progressive slope failure caused by  
 101 hydrate dissociation. The landslide is initiated on a finite length patch with slip-weakening  
 102 friction. The result can be used to extend the slope stability analysis with a convenient  
 103 corrector for progressive submarine landslide risk assessment.

## 104 **2 Initiation of progressive failure**

105 First we review the infinite slope model and then present the theoretical framework  
 106 for simulating the triggering of progressive slope failure, where the slip at the finite patch  
 107 reduces the friction and changes the shear stress.

### 108 **2.1 Infinite slope analysis**

109 If the sediment porosity is  $\phi$ , the saturated unit weight of the soil is  $\gamma = \rho_s(1 -$   
 110  $\phi)g + \rho_l\phi g$ , the unit weight of the water is  $\gamma_l = \rho_l g$ , and the submerged unit weight of  
 111 the soil is  $\gamma' = \gamma - \gamma_l$ . On the sliding interface with a dip angle  $\beta$ , the shear stress is  
 112 the destabilizing gravity component along the slope  $\tau_0 = \gamma'(H + D) \sin \beta \cos \beta$  where  
 113  $H$  is the depth below the seafloor to the hydrate layer of a thickness  $D$ , and  $\gamma'$  is the sub-  
 114 merged unit weight of the overlying layer. The failure surface is assumed to locate at the

base of the hydrate layer (Figure 1). The shear stress is balanced by the frictional re-

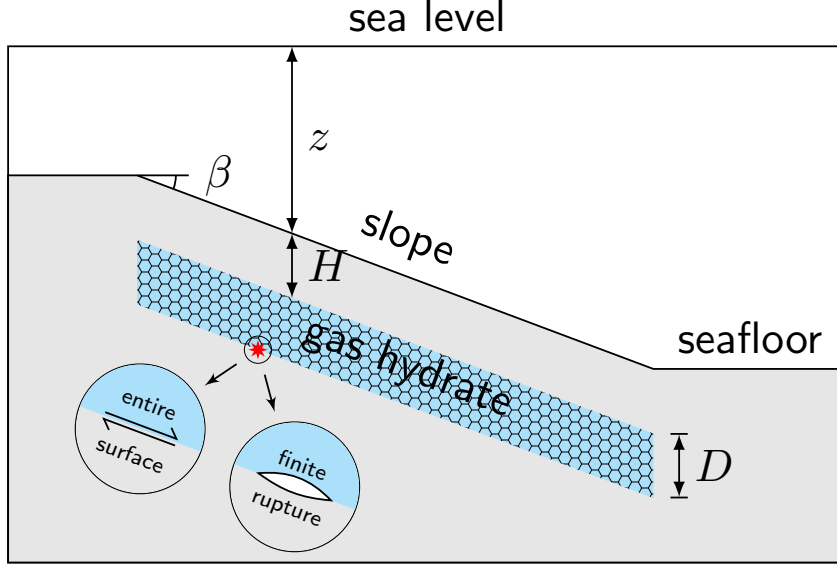


**Figure 1.** A schematic of the hydrate-bearing sediments on a submarine slope. The failure (labeled with a red star) occurs at the base of the hydrate layer of a thickness  $D$ , with an overlying sediment layer of a thickness  $H$ . The failure may be along the entire BHSZ, or start with a small rupture of a finite size.

115  
116 distance

$$117 \quad \tau_0 \leq c + f(\sigma_0 - \Delta u) \quad (1)$$

118 where  $c$  is the cohesion,  $f$  is the friction coefficient,  $\sigma_0 = \gamma'(H + D) \cos^2 \beta$  is the normal stress, and  $\Delta u$  is the excess pore pressure. With the entire failure surface sliding and  
119 the friction is taken as constant static friction  $\tan \psi$  where  $\psi$  is the friction angle, the  
120 safety factor is defined as (Duncan et al., 2014)  
121

$$122 \quad F_S = \frac{c + \tan \psi (\sigma_0 - \Delta u)}{\tau_0} = \frac{c + \tan \psi [\gamma'(H + D) \cos^2 \beta - \Delta u]}{\gamma'(H + D) \sin \beta \cos \beta}. \quad (2)$$

123 For unconsolidated sandy sediments,  $c$  is usually close to zero, and cementation caused  
124 by hydrates is neglected at low to moderate hydrate saturation. The hydrate in the pore  
125 spaces is assumed to have neutral buoyancy because the hydrate density is close to the  
126 pore water density. When  $F_S > 1$  the resisting forces are greater than the destabilizing  
127 forces, and the slope is considered stable. A slope is critically stable when  $F_S = 1$ ,  
128 but in practice the threshold of  $F_S$  is often taken to be slightly larger than unity (1.2  
129 or 1.5). The value  $F_S$  does not explicitly depend on the water depth because the con-  
130 tribution of water weight in the overburden is canceled out by the hydrostatic pore pres-  
131 sure.

132 The infinite slope analysis is typically employed in conventional slope failure as-  
133 sessment due to its simplicity. However, if the failure first occurs on a finite patch, the  
134 opening of the finite patch induces an additional term on the shear stress and alters the  
135 force balance.

## 136 2.2 Slip nucleation on a finite patch

137 The difference between the infinite slope model and the finite patch model is that  
 138 the former assumes that the slip occurs on the entire BHSZ, while the latter assumes that  
 139 the slip occurs on a finite patch. When a finite patch of a length  $2a$  at a sliding surface  
 140 far away from a free surface is set to slip, for cohesionless scenario the stress balance be-  
 141 comes (Viesca & Rice, 2012)

$$142 \quad f[\sigma_0 - \Delta u(x, t)] = \tau_0 - \frac{G}{2\pi(1-\nu)} \int_{-a}^a \frac{\partial \delta / \partial \xi \, d\xi}{x - \xi} \quad (3)$$

143 where  $\sigma_0$  and  $\tau_0$  are the same normal and shear stress caused by the effective weight of  
 144 the layer,  $\delta(x, t)$  is the slip distance on the patch,  $G$  is the shear modulus and  $\nu$  is the  
 145 Poisson ratio. Without the stress caused by the rupture, the cohesionless infinite slope  
 146 model is recovered. Equation (3) describes how the stress state on the potential sliding  
 147 surface is perturbed beyond the initial failed patch, and can be reduced to an eigenvalue  
 148 problem for  $V = d\delta/dt$  if we take into account the weakening of the frictional resis-  
 149 tance with  $\delta$  (Viesca & Rice, 2012) with a linear slip-weakening law

$$150 \quad f(\delta) = \tan \psi - \delta \Delta f / D_c \quad (4)$$

151 where  $\Delta f = \tan \psi - f_{ss}$  is the friction drop between the maximum static friction  $\tan \psi$   
 152 and the steady-state friction  $f_{ss}$ , and  $D_c$  is a characteristic length of the slip, typically  
 153 on the order of millimeters or centimeters as suggested by rock experiments (Rice & Ru-  
 154 ina, 1983; Marone, 1998). The eigenvalue problem gives a solution of the critical excess  
 155 pore pressure

$$156 \quad \Delta u_{\text{slip}} = \sigma_0 - \frac{\lambda_0 D_c G}{\Delta f a (1 - \nu)} \quad (5)$$

157 where  $\lambda_0 \approx 0.579$  is the smallest eigenvalue. Detailed description can be found in Viesca  
 158 and Rice (2012), and a brief derivation is provided in Appendix A.

159 The critical excess pore pressure  $\Delta u_{\text{slip}}$  required for slip nucleation depends on the  
 160 normal stress  $\sigma_0$ , the shear modulus  $G$ , the characteristic length  $D_c$ , the patch size  $a$ ,  
 161 and the friction drop  $\Delta f$ . Since for submarine landslides the steady-state friction coef-  
 162 ficient is  $f_{ss} \ll \tan \psi$ , the friction drop is  $\Delta f \approx \tan \psi$ , and the scaled crack size  $\chi =$   
 163  $a/D_c$  determines the critical excess pore pressure. The slip starts with a small slip with  
 164 respect to  $D_c$ , which is in the order of millimeters, and the minimal value of  $\chi$  is deter-  
 165 mined by setting  $\Delta u_{\text{slip}}$  to zero

$$166 \quad \chi_{\text{min}} = \frac{G \lambda_0}{\sigma_0 \Delta f (1 - \nu)}. \quad (6)$$

167 For a typical submarine slope with the slip located at a depth of  $\sim 100$  m below seafloor,  
 168 the shear modulus is  $G/(1-\nu) \sim 100$  MPa, the normal stress  $\sigma_0 \sim 1$  MPa, and the  
 169 value  $\chi_{\text{min}} \sim 10^2$ . The values of  $a$  and  $D_c$  are neither well constrained, but only their  
 170 ratio  $\chi$  appears in the results which is of the same order of magnitude as  $\chi_{\text{min}}$ , so we in-  
 171 corporate their uncertainties in  $\chi$ . The critical excess pore pressure  $\Delta u_{\text{slip}}$  can thus be  
 172 expressed as

$$173 \quad \Delta u_{\text{slip}} = \sigma_0 (1 - \chi_{\text{min}} / \chi). \quad (7)$$

174 It is clear that progressive failure may initiate when the safety factor  $F_S$  is still greater  
 175 than unity.

## 176 2.3 Overpressure caused by hydrate dissociation

177 Extensive studies exist to estimate the increase in pore pressure when the methane  
 178 hydrate dissociates (e.g., Xu & Germanovich, 2006; Kwon et al., 2008; Lee et al., 2010).  
 179 We follow the theoretical model developed by Xu and Germanovich (2006) to estimate

180 the overpressure. The excess pore pressure  $\Delta u$  from hydrate dissociation is related to  
 181 the hydrate dissociation rate as

$$182 \quad -\frac{R_v}{\kappa} \frac{dS_h}{dt} = \frac{\Delta u}{t_d} + \frac{d\Delta u}{dt} \quad (8)$$

183 where  $t$  is the time,  $R_v$  is the volume expansion factor depending on the saturation lev-  
 184 els of the liquid and gas phases (see Appendix B1 for details),  $S_h$  is the hydrate satu-  
 185 ration with an initial value  $S_h^0$ ,  $\kappa$  is the compressibility of the gas, hydrate, and liquid  
 186 solution at the three-phase equilibrium (Appendix B2), and  $t_d = \kappa\mu\phi DH/k$  is the char-  
 187 acteristic dissipation timescale determined by the effective permeability  $k$ , the viscos-  
 188 ity of the pore water  $\mu$ , the thickness of the dissociating hydrate layer  $D$ , and the depth  
 189 of the layer to the seafloor  $H$ . Note that  $\kappa$  is a function of  $S_h$  and the pore pressure  $P$ ,  
 190 which depends on both the overburden and compression caused by previously dissoci-  
 191 ated hydrate.

192 For a typical submarine hydrate reservoir,  $\kappa \sim 1 \text{ GPa}^{-1}$ ,  $\mu \sim 10^{-3} \text{ Pa} \cdot \text{s}$ ,  $DH \sim$   
 193  $10^4 \text{ m}^2$ ,  $k \sim 10^{-15} \text{ m}^2$ , so  $t_d \sim 10^7 \text{ s} \approx 0.3 \text{ yr}$ . A typical landslide occurs at a timescale  
 194  $t \ll t_d$ , in contrast with a slow sliding event which may last over a timescale much longer  
 195 than  $t_d$ , so the hydrate dissociates instantaneously and the flux out of the pores can be  
 196 ignored, which gives

$$197 \quad \Delta u = -R_v \int_{S_h^0}^{S_h} \frac{dS_h}{\kappa} \approx -\frac{R_v \Delta S_h}{\kappa(S_h^0)}. \quad (9)$$

198 where the approximation holds when  $\Delta S_h = S_h^0 - S_h \ll S_h^0$  and  $\kappa$  barely changes, so  
 199 the excess pore pressure is proportional to the amount of hydrate dissociated. Figure 2  
 200 shows how  $\Delta u$  varies with  $P$  and  $\Delta S_h$ . For  $\Delta u \leq 1 \text{ MPa}$ , the approximation is in good  
 201 agreement with  $\Delta u$  for a wide range of  $P$ , and we will use this approximation in the fol-  
 202 lowing analysis.

### 203 3 Applications to real submarine slopes

204 From eq. (5) we can calculate the excess pore pressure threshold for the cascad-  
 205 ing failure to occur on a submarine slope, and eq. (9) gives the amount of hydrate re-  
 206 quired to dissociate if the overpressure is caused by hydrate dissociation. To demonstrate  
 207 the difference between the infinite slope model and the progressive failure model, we first  
 208 apply the model to a hydrate site in the Shenhu region, Northern South China Sea, to  
 209 quantify the stability given the geological parameters, and next we use the model to ex-  
 210 plain the apparent high safety factors of the sites with landslides in the Ursa Basin, North-  
 211 ern Gulf of Mexico. The python scripts (Chen et al., 2023) are open-sourced under MIT  
 212 license.

#### 213 3.1 Shenhu Site GMGS3-W19, Northern South China Sea

214 Submarine landslides prevail in the continental slopes of the South China Sea from  
 215 Miocene to present times (Wang et al., 2018). The gas hydrate-bearing sediments at Site  
 216 GMGS3-W19, located in the Shenhu area in the Northern South China Sea, was stud-  
 217 ied in the third Chinese expedition in 2015. The parameters used in the model are listed  
 218 in Table 1. Among these parameters, the thickness of the hydrate layer  $D$  and the Pois-  
 219 son's ratio  $\nu$  are poorly constrained, and we use values of  $D$  and  $\nu$  within the inferred  
 220 range to calculate the critical values of  $\Delta u_{\text{slip}}$  and corresponding hydrate dissociation  
 221 amount  $\Delta S_h$ . The dissipation timescale is  $t_d \approx 50 \text{ d}$ , so for most landslides occurring  
 222 during a time period of a few days the instantaneous approximation eq. (9) can be used.  
 223 We choose a scaled patch size  $\chi = 100$ , and calculate three representative slope dip an-  
 224 gle values  $\beta = 5^\circ, 10^\circ$  and  $15^\circ$ . Clearly, variations in  $\chi$  play an important role in de-  
 225 termining the slope stability to progressive failure, and we will return to the effects of  
 226 variations in the Discussion section 4.1.

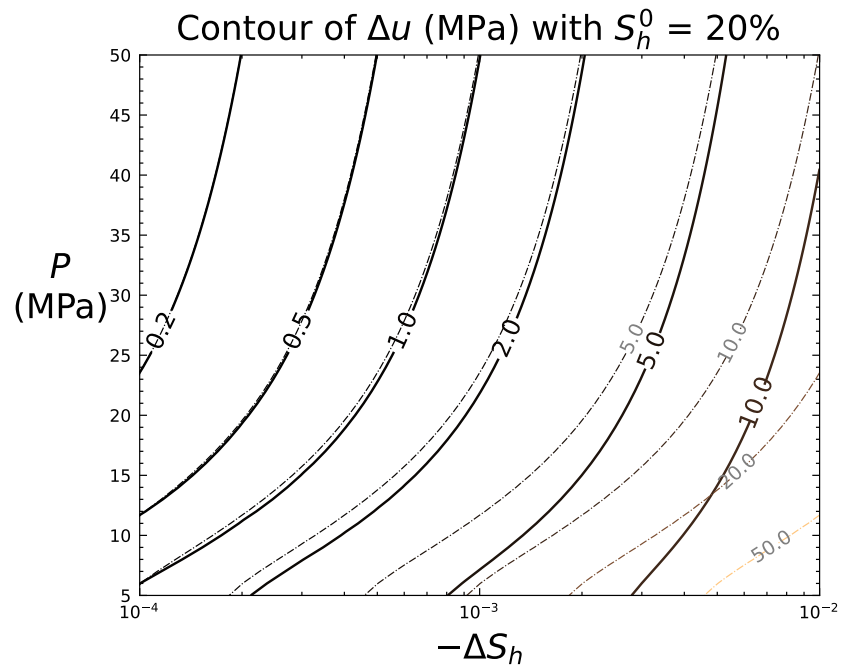


**Figure 2.** Excess pore pressure  $\Delta u$  caused by dissociation of hydrates with initial  $S_h^0 = 20\%$  in a confined initially gas-free pore following Xu and Germanovich (2006). The solid contour lines are calculated using the integration, whereas the dashed contour shows the approximation of the small dissociation, with gray  $\Delta u$  values labeling the levels with significant deviations. Clearly, the approximation matches the  $\Delta u$  well for  $\Delta u \leq 1$  MPa for a wide pressure range.

**Table 1.** Model parameters for the Shenhu hydrate site.

	Parameter	Symbol	Unit	Value
physical parameters	hydrate density <sup>a</sup>	$\rho_h$	kg/m <sup>3</sup>	929
	seawater density <sup>b</sup>	$\rho_l$	kg/m <sup>3</sup>	1029
	dry sediment density	$\rho_s$	kg/m <sup>3</sup>	2650
	molar mass of methane	$M$	g/mol	16.042
	methane mass fraction in hydrate	$x$	—	0.13
	water viscosity <sup>c</sup>	$\mu$	Pa·s	
geological parameters	water depth <sup>d</sup>	$z$	m	1273.8
	hydrate layer depth <sup>d</sup>	$H$	m	137.95
	maximum hydrate layer thickness <sup>d</sup>	$D$	m	17.6
	sediment porosity <sup>d</sup>	$\phi$	—	0.483
	intrinsic sediment permeability <sup>d</sup>	$k_0$	m <sup>2</sup>	$5.5 \times 10^{-15}$
	initial hydrate saturation <sup>d</sup>	$S_h^0$	—	0.452
	initial gas saturation <sup>d</sup>	$S_g^0$	—	0.194
	slope dip angle	$\beta$	°	
	friction angle <sup>d</sup>	$\psi$	°	25
	steady-state friction	$f_{ss}$	—	$\approx 0$
	Young's modulus <sup>d</sup>	$E$	MPa	70
	shear modulus <sup>d</sup>	$G$	MPa	$E/2(1 + \nu)$
	Poisson's ratio <sup>d</sup>	$\nu$	—	0.15–0.45

Sources: <sup>a</sup> Koh et al. (2011) <sup>b</sup> Spivey et al. (2004) <sup>c</sup> Straus and Schubert (1977)  
<sup>d</sup> Sum et al. (2017)

227 Figure 3 shows how  $\Delta u_{\text{slip}}$  and  $F_S$  vary with different  $D$ ,  $\nu$  and  $\beta$ , and the corre-  
228 sponding amount of hydrate dissociated to attain  $\Delta u_{\text{slip}}$ . In Figure 3a,  $\Delta u_{\text{slip}}$  increases  
229 with thicker  $D$ , smaller  $\beta$ , and smaller  $\nu$ . Mechanically, this indicates that if the BHSZ  
230 is deeper below the seafloor with a gentler slope and sediments easier to collapse, the risk  
231 of landslides is smaller. For the parameter ranges of interest, the excess pore pressure  
232 needed to initiate progressive failure is less than the critical pore pressure in the infinite  
233 slope model, indicated by the corresponding safety factor as high as 2.4 (Figure 3b). There-  
234 fore, the infinite slope model may overestimate the stability of the slope, and submarine  
235 landslides caused by progressive failure may occur on slopes that are previously consid-  
236 ered stable. Because  $\Delta u_{\text{slip}} \lesssim 1$  MPa, the corresponding amount of hydrate dissociated  
237 can be readily estimated using eq. (9), and the result is shown in Figure 3c with a simi-  
238 lar trend with the mechanical stability. For the parameters of Site GMGS3-W19, a change  
239 in  $S_h$  about 1 % is enough to destabilize the hydrate layer.

### 240 3.2 Ursa Basin, Northern Gulf of Mexico

241 Flemings et al. (2008) observed severe overpressure within 200 m below seafloor for  
242 sites U1322 and U1324 in the Ursa Basin in the Northern Gulf of Mexico, measured dur-  
243 ing Integrated Ocean Drilling Program (IODP) Expedition 308. The overpressure can  
244 reach 60 % of the hydrostatic effective stress  $\sigma'_{vh} = \gamma'(H+D)$  for Site U1324 and 70 %  
245 for Site U1322. Take Site U1324 for an example, the pore pressure satisfies

$$246 \frac{\Delta u}{\gamma'(H+D)} = \lambda^* \approx 0.6, \quad (10)$$

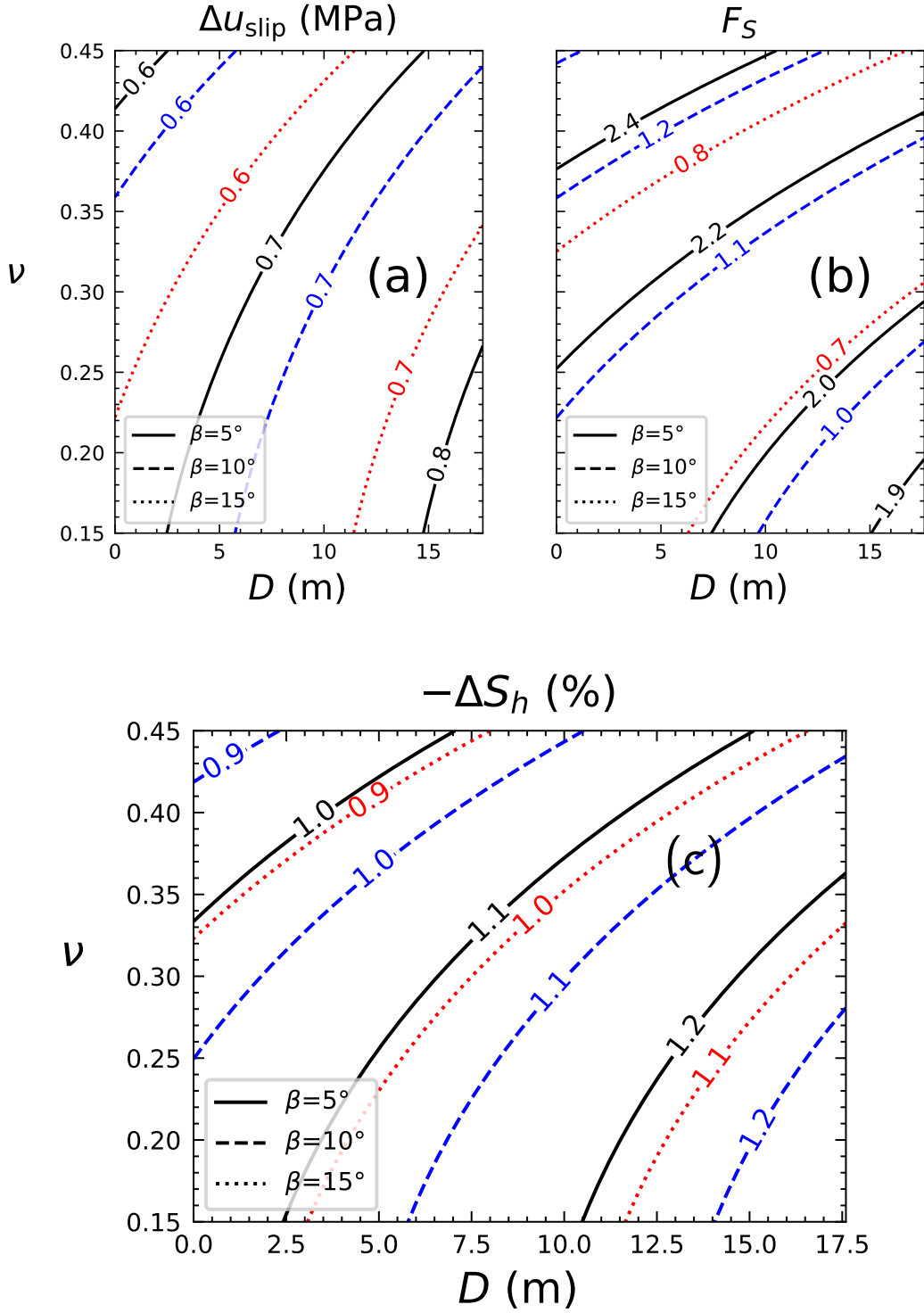


**Figure 3.** Contour plots of (a)  $\Delta u_{\text{slip}}$  with variations in  $D$  and  $\nu$ , (b) corresponding safety factor  $F_S$ , and (c) the amount of hydrate dissociated to generate  $\Delta u_{\text{slip}}$ . The styles of the contour lines denote the slope dip angle  $\beta$ . Smaller  $\nu$  and  $\beta$  and thicker  $D$  all contribute to higher  $\Delta u_{\text{slip}}$ , and more hydrate must dissociate to initiate progressive failure. An amount of about 1% is generally required. The solid, dotted and dashed contour lines are for the slope dip angles  $5^\circ$ ,  $10^\circ$  and  $15^\circ$ , respectively. The corresponding  $F_S$  when progressive failure starts are mostly greater than unity, and for the small  $\beta$  case,  $F_S$  may even exceed 2.4, a value so high that in the infinite slope model no landslide should occur.

247 and with a slope dip angle  $\beta = 2^\circ$  and friction angle  $\psi = 30^\circ$ , the safety factor is  $F_S \geq$   
 248 4.9, well above the critical value, which contrasts the fact that this site is prone to land-  
 249 slides. Infinite slope model allows limited options to reconcile this discrepancy: either  
 250 a higher overpressure up to  $0.93\sigma'_{vh}$  of the hydrostatic effective stress occurred during  
 251 the Pleistocene at the time of the landslide, or the site then had a much steeper slope  
 252 of  $10^\circ$ . Based on the geological evidence, neither explanation is well grounded.

253 A more straightforward explanation, however, is that the landslide is triggered by  
 254 progressive failure. The failure onset occurs when

$$255 \quad \gamma'(H + D) (\cos^2 \beta - \lambda^*) = \frac{\lambda_0 D_c G}{\Delta f a (1 - \nu)}. \quad (11)$$

256 Assuming a typical Poisson's ratio  $\nu = 0.3$ , Young's modulus  $E \sim 10$  MPa and fail-  
 257 ure depth at  $H+D \sim 200$  m, the scaled rupture patch size where failure occurs is  $\chi \approx$   
 258 8.4. For comparison,  $\chi_{\min} \approx 3.4$  can be calculated using the parameters. The initial  
 259 failure patch size  $2a$  is notably only one order of magnitude larger than  $D_c$ .

## 260 4 Discussion

### 261 4.1 Effect of the scaled rupture size

262 The scaled rupture size  $\chi = a/D_c$  is an important parameter in the slip nucle-  
 263 ation model because it relates the asperity-scale frictional property  $D_c$  to the macroscopic  
 264 rupture size  $a$ , but it is not well constrained. In modeling the site in Shenhu region we  
 265 have used  $\chi = 100$ , and  $\chi_{\min}$  can be calculated from eq. (6) to be around 35–50 for  
 266 the range of  $\nu$  and  $\beta$  provided in Table 1, which is on the same order of magnitude as  
 267  $\chi = 100$ . Similarly, for the sites in Ursa Basin,  $\chi_{\min} \approx 3.4$  is much smaller than that  
 268 of the site in Shenhu region, and as a result, the scaled rupture size  $\chi$  is accordingly re-  
 269 duced. Because  $\Delta u_{\text{slip}}$  can be expressed as

$$270 \quad \Delta u_{\text{slip}} = \sigma_0 (1 - \chi_{\min}/\chi), \quad (12)$$

271 a large  $\chi$  requires a higher overpressure closer to  $\sigma_0$ . In this study we generally choose  
 272  $\chi/\chi_{\min} \approx 2$ , consistent with the treatment in Viesca and Rice (2012) for the scenario  
 273 where the free surface is far from the sliding surface, i.e.,  $\sqrt{(H + D)/\chi_{\min} D_c} > 1$ .

### 274 4.2 Note on the friction laws

275 We use the slip-weakening friction in the model because it is easy to derive the eigen-  
 276 value problem from the force balance. However, the result is not limited by the exact  
 277 form of the friction laws as long as the friction drops as sliding, and we can also use the  
 278 rate-weakening friction to derive similar results. For example, the Dieterich-Ruina fric-  
 279 tion constitutive law (Dieterich, 1979; Ruina, 1983) is

$$280 \quad f = f_0 + A \ln \frac{V}{V_0} + B \ln \frac{V_0 \theta}{L}, \quad \frac{d\theta}{dt} = 1 - \frac{V\theta}{L} \quad (13)$$

281 where  $V$  is the sliding velocity,  $\theta$  is a state variable representing the sliding history,  $L$   
 282 is a characteristic length scale,  $f_0$  is the reference friction,  $V_0$  is the reference velocity,  
 283 and  $A$  and  $B$  are constants. Substitute the friction in eq. (3) and take the time deriva-  
 284 tive, we have

$$285 \quad \left( A \frac{\dot{V}}{V} + B \frac{\dot{\theta}}{\theta} \right) (\sigma_0 - \Delta u) = -\frac{G}{2\pi(1-\nu)} \int_{-a}^a \frac{\partial V(\xi, t)}{\partial \xi} \frac{d\xi}{x - \xi}. \quad (14)$$

286 After scaling with  $V_{\text{rms}}$  and keeping only the leading order of  $V$ , the equation becomes  
 287 the same as using the slip-weakening friction.

## 288 5 Conclusion

289 In this study, we have shown that the infinite slope model may overestimate the  
 290 stability of submarine slopes, and the progressive failure model can be used to assess the  
 291 risk of submarine landslides. The critical excess pore pressure required to initiate pro-  
 292 gressive failure is generally less than 1 MPa, and the corresponding amount of hydrate  
 293 dissociated is  $\sim 1\%$ , which is much smaller than the critical pore pressure in the infi-  
 294 nite slope model. On a potential failure surface deeper below the seafloor, with a gen-  
 295 tler slope and more easily collapsing sediments, the overpressure required to initiate pro-  
 296 gressive failure is greater and the risk of landslides is lower. The critical excess pore pres-  
 297 sure is also affected by the scaled rupture size  $\chi = a/D_c$ , which is not well constrained  
 298 but is on the same order of magnitude with  $\chi_{\min} = 0.579G/\sigma_0\Delta f(1 - \nu)$ . For some  
 299 landslide sites where infinite slope analysis gives unrealistically high safety factors, the  
 300 progressive failure model provides a more reasonable explanation.

## 301 6 Open Research

302 The python scripts of the model are available at [https://gitlab.com/jzchenjz/](https://gitlab.com/jzchenjz/hydrate-induced-progressive-landslides)  
 303 `hydrate-induced-progressive-landslides`, open-sourced under MIT license.

## 304 Appendix A Landslide with slip-weakening friction

### 305 A1 Finite length rupture model

306 For a finite rupture patch located between  $x = \pm a$  far from the free surface, fol-  
 307 low the treatment of Viesca and Rice (2012) after scaling the spatial coordinates to place  
 308 the rupture patch between  $x = \pm 1$  we obtain

$$309 \frac{\Delta fa(1 - \nu)}{D_c G} \left( \frac{\tau_0}{\tan \psi} - \Delta u \right) V = \frac{1}{2\pi} \int_{-1}^{+1} \frac{\partial V / \partial s}{x - s} ds \quad (\text{A1})$$

310 where  $V$  is  $d\delta/dt$  scaled by its RMS value. At the boundaries of the rupture,  $V(\pm 1) =$   
 311  $0$ . The equation becomes an eigenvalue problem

$$312 \lambda V(x) = \frac{1}{2\pi} \int_{-1}^1 \frac{V'(s)}{x - s} ds, \quad (\text{A2})$$

313 where the eigenvalue is

$$314 \lambda = \frac{\Delta fa(1 - \nu)}{D_c G} \left( \frac{\tau_0}{\tan \psi} - \Delta u \right) \quad (\text{A3})$$

315 and the smallest eigenvalue  $\lambda_0$  corresponds to the nucleation of the rupture with min-  
 316 imum pore pressure increase. From eq. (A2) we can obtain

$$317 \lambda V(x) = -\frac{1}{2\pi} \int_{-1}^1 V(y) \frac{d}{dy} \frac{1}{x - y} dy, \quad (\text{A4})$$

318 and with a uniform spacing  $h = 1/N$ , where  $2N + 1$  is the number of grid points on  
 319  $[-1, 1]$  we get

$$320 \lambda V(x_i) \approx -\frac{h}{2\pi} \sum_{j=-N}^N V(x_j) \left( \frac{d}{dy} \frac{1}{x_i - y} \right) \Big|_{y=x_j} = -\frac{1}{2\pi} \sum_{j=-N}^N V(x_j) \left( \frac{1}{x_i - x_{j+1/2}} - \frac{1}{x_i - x_{j-1/2}} \right) \\ = -\frac{h}{2\pi} \sum_{j=-N}^N \frac{V(x_j)}{(x_i - x_j)^2 - h^2/4} \quad (\text{A5})$$

321 or with  $V_i = V(x_i)$

$$322 \quad \lambda V_i = -\frac{N}{2\pi} \sum_{j=-N}^N \frac{V_j}{(i-j)^2 - 1/4}, \quad (\text{A6})$$

323 which can be written in a matrix form

$$324 \quad \lambda V = KV \quad (\text{A7})$$

325 where  $V = (V_{-N}, V_{-N+1}, \dots, V_{N-1}, V_N)^\top$  and  $K$  is a symmetric matrix

$$326 \quad K_{ij} = -\frac{N}{2\pi[(i-j)^2 - 1/4]} \quad (\text{A8})$$

327 with  $2N + 1$  real eigenvalues. The matrix is strictly diagonally dominant

$$328 \quad |K_{ii}| > \sum_{j \neq i} |K_{ij}| \quad (\text{A9})$$

329 and all diagonal elements are positive, so the eigenvalues are all positive by the Gershgorin circle theorem. The smallest eigenvalue is  $\lambda_0 \approx 0.579$ . The excess pore pressure  
330 is related to the crack length as  
331

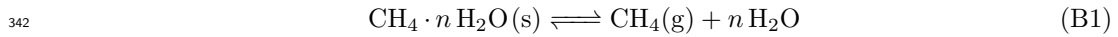
$$332 \quad \Delta u_{\text{slip}} = \frac{\tau_0}{\tan \psi} - \frac{\lambda_0 D_c G}{\Delta f a (1 - \nu)}. \quad (\text{A10})$$

333 With an estimate of  $a/D_c$ , we can predict if the excess pore pressure  $\Delta u$  can cause a land-  
334 slide.

## 335 **Appendix B overpressurization due to hydrate dissociation**

### 336 **B1 Expansion factor**

337 The density of methane hydrate is smaller than the density of water, so if there is  
338 no gaseous phase released during hydrate dissociation (i.e., hydrate dissolution), no ex-  
339 cess pore pressure is generated. With negligible methane solubility in the pore water,  
340 with no gas phase present, the relative volume change to the pore volume in the reac-  
341 tion



343 is

$$344 \quad \frac{V_d}{V_p} = \frac{\Delta V_l + \Delta V_h + \Delta V_g}{V_p} = \frac{\Delta V_l + \Delta V_h + \Delta V_g}{\Delta V_h} \Delta S_h \quad (\text{B2})$$

345 where  $V_d$  is the volume change during the dissociation assuming no pressure and tem-  
346 perature change,  $V_p$  is the pore volume,  $\Delta S_h$  is the change of pore volume hydrate frac-  
347 tion, and subscripts w, h and g denote the pore water, the hydrates and the free methane  
348 gas. The mass fraction of methane in the hydrate is treated as a constant  $x$ , close to 0.13  
349 for an ideal hydration number  $n = 5.75$ , so the relations between the volume changes  
350 are

$$351 \quad \Delta V_g = -\frac{x\rho_h}{\rho_g} \Delta V_h, \quad \Delta V_l = -\frac{(1-x)\rho_h}{\rho_l} \Delta V_h \quad (\text{B3})$$

352 and the total volume change relative to the pore volume  $V_p$  is  $V_d/V_p = -R_v \Delta S_h$  where  
353 the volume expansion factor  $R_v$  is

$$354 \quad R_v = (1-x)\rho_h/\rho_l + x\rho_h/\rho_g - 1. \quad (\text{B4})$$

355 The density of the hydrate can be treated as constant, and the pore water density can  
356 be calculated using Spivey et al. (2004). The density of the methane gas is calculated  
357 using an appropriate equation of state for methane, e.g., Setzmann and Wagner (1991).

358 In some works (e.g., Nixon & Grozic, 2007),  $R_v$  is simplified using  $\rho_h/\rho_l \approx 1$  and the  
 359 ideal gas approximation

$$360 \quad R_v \approx \frac{x\rho_h}{\rho_g} - x = 164.6 \frac{T_e P^\circ}{T^\circ P} - 0.13 \quad (\text{B5})$$

361 where  $T_e$  is the equilibrium temperature of the gas hydrate in Kelvin and  $P$  is the pres-  
 362 sure in atm. The volume ratio 164.6 is calculated under a standard condition  $P^\circ = 1$  atm  
 363 and  $T^\circ = 273.15$  K.

## 364 **B2 Total compressibility**

365 We have calculated the volume expansion factor, which assumes constant temper-  
 366 ature and pressure during the dissociation. However, the expanded volume is confined  
 367 in the pore space. If the pores are taken as rigid, the additional liquid and gas must be  
 368 compressed. The compressibility  $\kappa$  can be approximated in different means. For exam-  
 369 ple, Nixon and Grozic (2007) used relations between the void ratio  $e = \phi/(1 - \phi)$ , the  
 370 effective stress  $\sigma'$ , and empirically determined soil swelling index  $C_s$ . Xu and Germanovich  
 371 (2006) avoided the empirical treatment using

$$372 \quad \kappa = -\frac{1}{V} \frac{dV}{dP} = -\frac{1}{V} \left( \frac{\partial V}{\partial P} + \frac{\partial V}{\partial T_e} \frac{dT_e}{dP} \right) = \sum_i \frac{S_i}{\rho_i} \left( \frac{\partial \rho_i}{\partial P} + \frac{\partial \rho_i}{\partial T_e} \frac{dT_e}{dP} \right) = \kappa_g S_g + \kappa_l S_l \quad (\text{B6})$$

373 where  $S_i$  is the saturation of the  $i$ -th component,  $\rho_i$  is the density of the  $i$ -th component,  
 374 and  $T_e$  is the three-phase equilibrium temperature. The pressure and temperature de-  
 375 pendence of the hydrate density is neglected, and the compressibility factors of the gas  
 376 and liquid phases are

$$377 \quad \kappa_g = \frac{1}{\rho_g} \left( \frac{\partial \rho_g}{\partial P} + \frac{T_e^2 R}{P \Delta H_m} \frac{\partial \rho_g}{\partial T_e} \right), \quad \kappa_l = \frac{1}{\rho_l} \left( \frac{\partial \rho_l}{\partial P} + \frac{T_e^2 R}{P \Delta H_m} \frac{\partial \rho_l}{\partial T_e} \right) \quad (\text{B7})$$

378 where the Clapeyron-Clausius equation  $dT_e/dP = T_e^2 R/(P \Delta H_m)$  is used, and  $\Delta H_m =$   
 379  $54.44$  kJ/mol (Gupta et al., 2008) is the latent heat of methane hydrate dissociation. When  
 380 calculating  $\kappa$ , we tested both Setzmann and Wagner (1991) and simpler Peng and Robin-  
 381 son (1976) models to calculate the methane gas density. The results are almost the same.

## 382 **B3 Excess pore pressure in confined pores**

383 In a confined pore of a volume  $V_p$  with saturation levels  $S_g$ ,  $S_l$ , and  $S_h = 1 - S_g -$   
 384  $S_l$ , when the hydrate saturation changes by  $dS_h$  and results in a pressure change  $dP$ ,  
 385 the changes in  $S_g$  and  $S_l$  are

$$386 \quad dS_g = -\frac{\rho_h}{\rho_g} x dS_h - \kappa_g S_g dP, \quad dS_l = -\frac{\rho_h}{\rho_l} (1 - x) dS_h - \kappa_l S_l dP. \quad (\text{B8})$$

387 Add the two equations and substitute  $dS_h = -dS_g - dS_l$ , and we arrive at

$$388 \quad \kappa dP = -R_v dS_h. \quad (\text{B9})$$

389 The differential equations to solve are

$$390 \quad \frac{dP}{dS_h} = -\frac{R_v}{\kappa} \quad (\text{B10})$$

$$391 \quad \frac{dS_g}{dS_h} = -\frac{\rho_h}{\rho_g} x - \kappa_g \frac{dP}{dS_h} \quad (\text{B11})$$

392 During the dissociation, the pressure increases, so both  $R_v$  and  $\kappa$  are also changing. The  
 393 equations are solved iteratively. Figure 2 shows the diagram of  $\Delta u$  with change of hy-  
 394 drate saturation and pressure.

395 **Acknowledgments**

396 This research is funded by National Key R&D Program of China (NO.2022YFC2805503),  
397 and Key Research and Development Program of Hainan Province, China (No. ZDYF2020209).

398 **References**

- 399 Berndt, C., Costa, S., Canals, M., Camerlenghi, A., De Mol, B., Saunders, M.,  
400 & Shearer, P. (2012, February 21). Repeated slope failure linked to fluid  
401 migration: The ana submarine landslide complex, eivissa channel, west-  
402 ern mediterranean sea. *Earth Planet. Sci. Lett.*, *319-320*, 65–74. doi:  
403 10.1016/j.epsl.2011.11.045
- 404 Brothers, D. S., Luttrell, K. M., & Chaytor, J. D. (2013, September). Sea-  
405 level-induced seismicity and submarine landslide occurrence. *Geology*, *41*(9),  
406 979–982. doi: 10.1130/g34410.1
- 407 Brown, H. E., Holbrook, W. S., Hornbach, M. J., & Nealon, J. (2006, June).  
408 Slide structure and role of gas hydrate at the northern boundary of the  
409 storegga slide, offshore norway. *Mar. Geol.*, *229*(3-4), 179–186. doi:  
410 10.1016/j.margeo.2006.03.011
- 411 Chen, J., Mei, S., Wang, D., Sun, J., & Sun, Y. (2023).  
412 <https://gitlab.com/jzchenjz/hydrate-induced-progressive-landslides>.
- 413 Dieterich, J. H. (1979). Modeling of rock friction .1. experimental results and con-  
414 stitutive equations. *J. Geophys. Res.*, *84*(Nb5), 2161–2168. doi: 10.1029/  
415 JB084iB05p02161
- 416 Duncan, J. M., Wright, S. G., & Brandon, T. L. (2014). *Soil strength and slope sta-*  
417 *bility*. John Wiley & Sons, Inc.
- 418 Flemings, P., Long, H., Dugan, B., Germaine, J., John, C., Behrmann, J., & Sawyer,  
419 D. (2008, May). Pore pressure penetrometers document high overpressure  
420 near the seafloor where multiple submarine landslides have occurred on the  
421 continental slope, offshore louisiana, gulf of mexico. *Earth Planet. Sci. Lett.*,  
422 *269*(3-4), 309–325. doi: 10.1016/j.epsl.2007.12.005
- 423 Ginsburg, G. D., Soloviev, V. A., et al. (1995). Submarine gas hydrate estimation:  
424 theoretical and empirical approaches. In *Offshore technology conference*. doi:  
425 10.4043/7693-ms
- 426 Gupta, A., Lachance, J., Sloan, E. D., & Koh, C. A. (2008, December). Mea-  
427 surements of methane hydrate heat of dissociation using high pressure dif-  
428 ferential scanning calorimetry. *Chem. Eng. Sci.*, *63*(24), 5848–5853. doi:  
429 10.1016/j.ces.2008.09.002
- 430 Kayen, R. E., & Lee, H. J. (1991, January). Pleistocene slope instability of gas  
431 hydrate-laden sediment on the beaufort sea margin. *Mar. Geotechnol.*, *10*(1-2),  
432 125–141. doi: 10.1080/10641199109379886
- 433 Koh, C. A., Sloan, E. D., Sum, A. K., & Wu, D. T. (2011, July). Fundamentals and  
434 applications of gas hydrates. *Annu. Rev. Chem. Biomol.*, *2*(1), 237–257. doi:  
435 10.1146/annurev-chembioeng-061010-114152
- 436 Kvenvolden, K. A. (1988, December). Methane hydrate—a major reservoir of car-  
437 bon in the shallow geosphere? *Chem. Geol.*, *71*(1-3), 41–51. doi: 10.1016/0009-  
438 -2541(88)90104-0
- 439 Kwon, T.-H., Cho, G.-C., & Santamarina, J. C. (2008, March). Gas hydrate dis-  
440 sociation in sediments: Pressure-temperature evolution. *Geochem. Geophys.*  
441 *Geosyst.*, *9*(3), Q03019. doi: 10.1029/2007gc001920
- 442 Lafuerza, S., Sultan, N., Canals, M., Lastras, G., Cattaneo, A., Frigola, J., ...  
443 Berndt, C. (2012, April). Failure mechanisms of ana slide from geotechni-  
444 cal evidence, eivissa channel, western mediterranean sea. *Mar. Geol.*, *307-310*,  
445 1–21. doi: 10.1016/j.margeo.2012.02.010
- 446 Lee, J. Y., Santamarina, J. C., & Ruppel, C. (2010, March). Volume change asso-

- 447 ciated with formation and dissociation of hydrate in sediment. *Geochem. Geo-*  
 448 *phys. Geosyst.*, 11(3). doi: 10.1029/2009gc002667
- 449 Marone, C. (1998, May). Laboratory-derived friction laws and their application to  
 450 seismic faulting. *Annu. Rev. Earth Planet. Sci.*, 26(1), 643–696. doi: 10.1146/  
 451 annurev.earth.26.1.643
- 452 Maslin, M., Owen, M., Betts, R., Day, S., Jones, T. D., & Ridgwell, A. (2010, April).  
 453 Gas hydrates: past and future geohazard? *Philos. Trans. R. Soc. London, Ser.*  
 454 *A*, 368(1919), 2369–2393. doi: 10.1098/rsta.2010.0065
- 455 Nixon, M. F., & Grozic, J. L. H. (2007, March). Submarine slope failure due to  
 456 gas hydrate dissociation: a preliminary quantification. *Can. Geotech. J.*, 44(3),  
 457 314–325. doi: 10.1139/t06-121
- 458 Normandeau, A., MacKillop, K., Macquarrie, M., Richards, C., Bourgault, D.,  
 459 Campbell, D. C., ... Clarke, J. H. (2021, June). Submarine landslides trig-  
 460 gered by iceberg collision with the seafloor. *Nat. Geosci.*, 14(8), 599–605. doi:  
 461 10.1038/s41561-021-00767-4
- 462 Peng, D.-Y., & Robinson, D. B. (1976, February). A new two-constant equation of  
 463 state. *Ind. Eng. Chem. Fundam.*, 15(1), 59–64. doi: 10.1021/i160057a011
- 464 Riboulot, V., Cattaneo, A., Sultan, N., Garziglia, S., Ker, S., Imbert, P., & Voisset,  
 465 M. (2013, August). Sea-level change and free gas occurrence influencing a  
 466 submarine landslide and pockmark formation and distribution in deepwater  
 467 nigeria. *Earth Planet. Sci. Lett.*, 375, 78–91. doi: 10.1016/j.epsl.2013.05.013
- 468 Rice, J. R., & Ruina, A. L. (1983, June). Stability of steady frictional slipping. *J.*  
 469 *Appl. Mech.*, 50(2), 343. doi: 10.1115/1.3167042
- 470 Ruina, A. (1983, December). Slip instability and state variable friction laws. *J. Geo-*  
 471 *phys. Res.*, 88(Nb12), 10359–10370. doi: 10.1029/jb088ib12p10359
- 472 Setzmann, U., & Wagner, W. (1991, November). A new equation of state and tables  
 473 of thermodynamic properties for methane covering the range from the melting  
 474 line to 625 k at pressures up to 100 MPa. *J. Phys. Chem. Ref. Data*, 20(6),  
 475 1061–1155. doi: 10.1063/1.555898
- 476 Sloan, E. D., & Koh, C. (2007). *Clathrate hydrates of natural gases*. CRC press.
- 477 Smith, D., Harrison, S., & Jordan, J. (2013, December). Sea level rise and sub-  
 478 marine mass failures on open continental margins. *Quat. Sci. Rev.*, 82, 93–103.  
 479 doi: 10.1016/j.quascirev.2013.10.012
- 480 Spivey, J. P., McCain, W. D., & North, R. (2004, July). Estimating density, forma-  
 481 tion volume factor, compressibility, methane solubility, and viscosity for oilfield  
 482 brines at temperatures from 0 to 275 °c, pressures to 200 MPa, and salinities  
 483 to 5.7 mole/kg. *J. Can. Pet. Technol.*, 43(07). doi: 10.2118/04-07-05
- 484 Straus, J. M., & Schubert, G. (1977, January). Thermal convection of water in  
 485 a porous medium: Effects of temperature- and pressure-dependent thermo-  
 486 dynamic and transport properties. *J. Geophys. Res.*, 82(2), 325–333. doi:  
 487 10.1029/jb082i002p00325
- 488 Sultan, N., Cochonat, P., Foucher, J.-P., & Mienert, J. (2004, December). Effect  
 489 of gas hydrates melting on seafloor slope instability. *Mar. Geol.*, 213(1-4), 379–  
 490 401. doi: 10.1016/j.margeo.2004.10.015
- 491 Sun, J., Zhang, L., Ning, F., Lei, H., Liu, T., Hu, G., ... Wu, N. (2017, Septem-  
 492 ber). Production potential and stability of hydrate-bearing sediments at the  
 493 site GMGS3-w19 in the south china sea: A preliminary feasibility study. *Mar.*  
 494 *Petrol. Geol.*, 86, 447–473. doi: 10.1016/j.marpetgeo.2017.05.037
- 495 Viesca, R. C., & Rice, J. R. (2012, March). Nucleation of slip-weakening rupture  
 496 instability in landslides by localized increase of pore pressure. *J. Geophys. Res.*  
 497 *Solid Earth*, 117(B3), 1–21. doi: 10.1029/2011JB008866
- 498 Wang, W., Wang, D., Wu, S., Völker, D., Zeng, H., Cai, G., & Li, Q. (2018, Jan-  
 499 uary). Submarine landslides on the north continental slope of the south china  
 500 sea. *J. Ocean Univ. China*, 17(1), 83–100. doi: 10.1007/s11802-018-3491-0
- 501 Xu, W., & Germanovich, L. N. (2006, January). Excess pore pressure resulting from

502 methane hydrate dissociation in marine sediments: A theoretical approach. *J.*  
503 *Geophys. Res.*, 111(B1). doi: 10.1029/2004jb003600

Figure 1.

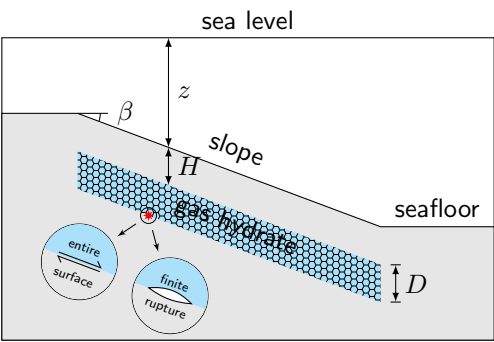


Figure 2.

# Contour of $\Delta u$ (MPa) with $S_h^0 = 20\%$

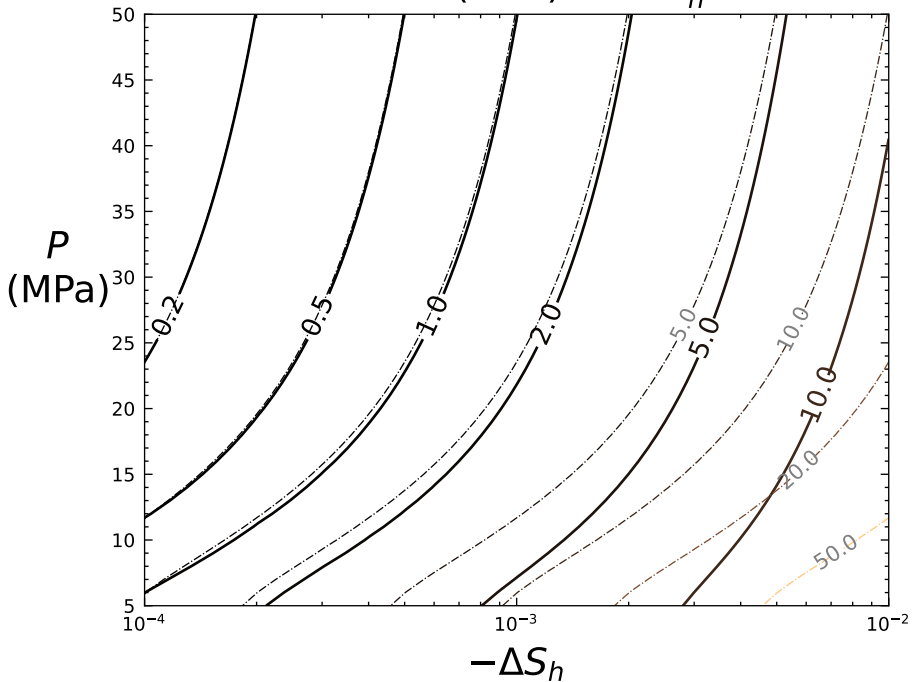


Figure 3.

